

---

This is an electronic reprint of the original article.  
This reprint may differ from the original in pagination and typographic detail.

Keitaanniemi, Aino; Rönholm, Petri; Kukko, Antero; Vaaja, Matti Tapio

## Drift analysis and sectional post-processing of indoor simultaneous localization and mapping (SLAM)-based laser scanning data

*Published in:*  
Automation in Construction

*DOI:*  
[10.1016/j.autcon.2022.104700](https://doi.org/10.1016/j.autcon.2022.104700)

Published: 01/03/2023

*Document Version*  
Publisher's PDF, also known as Version of record

*Published under the following license:*  
CC BY

*Please cite the original version:*  
Keitaanniemi, A., Rönholm, P., Kukko, A., & Vaaja, M. T. (2023). Drift analysis and sectional post-processing of indoor simultaneous localization and mapping (SLAM)-based laser scanning data. *Automation in Construction*, 147, Article 104700. <https://doi.org/10.1016/j.autcon.2022.104700>

---

This material is protected by copyright and other intellectual property rights, and duplication or sale of all or part of any of the repository collections is not permitted, except that material may be duplicated by you for your research use or educational purposes in electronic or print form. You must obtain permission for any other use. Electronic or print copies may not be offered, whether for sale or otherwise to anyone who is not an authorised user.



# Drift analysis and sectional post-processing of indoor simultaneous localization and mapping (SLAM)-based laser scanning data

Aino Keitaanniemi <sup>a,\*</sup>, Petri Rönholm <sup>a</sup>, Antero Kukko <sup>a,b</sup>, Matti T. Vaaja <sup>a</sup>

<sup>a</sup> Department of Built Environment, School of Engineering, Aalto University, Otakaari 4, P.O. Box 14100, Aalto, 00076, Finland

<sup>b</sup> Finnish Geospatial Research Institute FGI, Geodeetinrinne 2, Masala, 02430, Finland

## ABSTRACT

Even though the SLAM laser scanners (LSs) have the required resolution for construction analysis, a drift error has been detected in georeferencing phase of the data processing. The reduction of drift error in SLAM LSs with third-party software has not been studied. This paper demonstrates the drift error behavior of commercial SLAM LSs and their correction with sectional post-processing methods, and shows that the drift error is mainly in a vertical direction, and it is largest in the middle of the trajectory. The drift error was reduced from 10.6 cm to 0.2 cm. Circa 30 s length sections have better results than larger sections with non-rigid transformation algorithm. The method has shown potential to improve the quality and cost-effectiveness of multitemporal construction documentation. In addition, locations of additional control points were analyzed to prevent drift error, with adjustments to the walking path.

## 1. Introduction

3D data such as point clouds have been part of the construction industry for almost two decades [1]. It has been used for example in construction monitoring and quality control. Even though the full automation of these applications is still a challenge it is known that a combination of sensors is required to overcome the challenge [2]. In addition, the integration of multiple data sources can improve the effectiveness of construction site documentation [3,4]. Photogrammetry sensors and cameras as well as static laser scanners (LSs) have been used in the construction industry [5]. Besides these sensors, it has been proven that handheld SLAM LSs have the required resolution for construction analysis. In addition, the usage of handheld sensors does not need trained users, and walking in the site is enough to capture the environment [6].

In addition to construction applications, handheld SLAM LSs have been studied in other applications such as cultural heritage modeling (e.g. [7,8]), underground mine mapping (e.g. [9,10]), building interior modeling (e.g. [11,12]), landform mapping (e.g. [13,14]), and tree modeling [15]. There have been reports of detections of drift errors in SLAM point clouds. In the Raval et al. [16] study, a drift that is larger than a meter occurred during a one-kilometer closed-loop measurement in an underground mine. Correspondingly, Frangez et al. [10] detected the drift in an underground mine during line measurement. Zlot et al. [17] noticed that a drift error can be from 10 cm to over 1 m between features that are over 100 m apart in an outdoor cultural heritage site. In addition, in our earlier study, we detected a 20–40 cm drift during measurements on a straight street side [18].

The common feature of these studies is that the drift error was detected after the data was fitted to ground control by georeferencing [10,16–18]. The reason for the late detection is that the processing of the point cloud is done after the data collection and for this reason the users were unaware of problems during the SLAM data collection. Another common feature of these studies is that the drift error is small at the beginning of the trajectories, and it grows over time. However, the local error of the SLAM point clouds is minimal because the features in the environment are detected correctly, meaning that elements such as small rooms and the features inside them are in scale [10,16–18]. For these reasons, it is hard to recognize the drift error without georeferencing.

3D data has been used for many applications in the construction industry such as quality inspections, progress tracking and construction automation [1]. The analyses are possible when a construction site has multi-time 3D data or a building information model (BIM) as a reference. However, the data should not have any drift if the analysis is meant to be reliable. For example, change detection between a drifted SLAM point cloud and a terrestrial laser scanning point cloud can demonstrate changes that do not exist in the environment. It is essential to reduce the effect of SLAM point cloud drifting if the purpose of the analysis is to apply it for construction purposes.

Errors in SLAM laser scanning have been reduced by improving the SLAM algorithm (e.g., [19,20]). This is not possible for the user of commercial SLAM LSs which utilize mostly black box SLAM algorithms. The authors have not found any studies that cover the impact of reducing errors with post-processing in commercial SLAM LSs. The

\* Corresponding author.

E-mail address: [aino.keitaanniemi@aalto.fi](mailto:aino.keitaanniemi@aalto.fi) (A. Keitaanniemi).

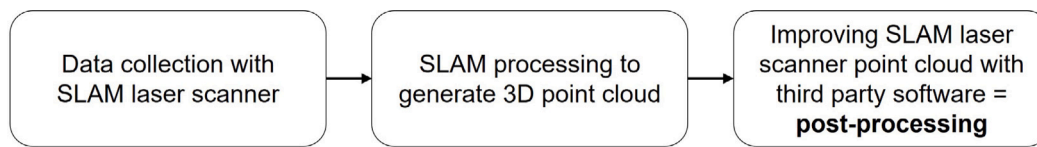


Fig. 1. Definition of post-processing used in this manuscript.

definition of post-processing in this manuscript is illustrated in Fig. 1. Before post-processing, the SLAM point cloud is collected with a SLAM LS and processed into a point cloud in the scanner's software. Then the point cloud is typically improved in third-party software. This includes noise removal, georeferencing, and error reduction with correction algorithms.

Differing from SLAM, drift errors have been reduced during post-processing in traditional mobile laser scanning (MLS), in which case the calculation of the measurement trajectory is based on GNSS-IMU positioning (global navigation satellite system and inertial measurement unit). The reduction can be executed with a data-driven method or a model-driven method. The data-driven method reduces error based on ground control points and correction algorithms. The model-driven method reduces error based on mathematical models of MLS and analyzes individual error sources [21]. Both of the methods have been widely used with traditional MLS [22–32]. There is also plenty of software where this kind of error reduction is possible to execute [30, 33,34]. Because SLAM laser scanning has similar features to traditional MLS, these methods could be utilized in SLAM laser scanning. In addition, the post-processing of the traditional MLS as well as the SLAM point cloud could be executed in sections (later sectional post-processing). In case of SLAM point clouds, the sections can be created based on the timestamps that the SLAM LS collects for the points.

This study aims to demonstrate error behavior and correction in drifted SLAM point clouds of the commercial SLAM laser scanner and software. The hypothesis regarding drift error behavior in SLAM point clouds is that the error is largest in the areas that are furthest from the start and end location in a loop measurement. In addition, we executed an experimental study on how much post-processing can reduce drift errors when the reduction of the error is done section-wise regarding the SLAM point cloud. This is executed with datasets with SLAM LS and terrestrial LS of building interiors and a small section in front of a building. The hypothesis of sectional error reduction is that smaller sections may decrease the error more than larger sections.

## 2. SLAM algorithms and drifting

Several SLAM algorithms exist. However, they have some repeating features. Every SLAM algorithm solves the problem of locating the sensor inside an unknown environment without knowledge of its own location. The basic process of the SLAM algorithm is building a map of an environment and at the same time using this map for locating itself. For this, a SLAM algorithm estimates the location of the sensor and the locations of the landmarks. At every timestamp, the algorithm saves the correlations between the sensor and the landmarks. The SLAM algorithm then updates the map and sensor locations.[35]. To get good precision on the mapping results, SLAM algorithms require a closed-loop survey [36]. The most known SLAM algorithms are Extended Kalman Filter (EKF) SLAM and Rao-Blackwellized particle filter known as FastSLAM [35]. The new generation of the SLAM algorithms are based on the factor graphs, and they have been implemented in studies [37,38].

Most of the SLAM algorithms extract and match the features of two consecutive point cloud sets of different timestamps. Then they calculate the relative motion distance and location change with the IMU. This combination will solve the position of the SLAM laser scanner itself. The mathematical calculations differ in the algorithms [39].

Another possible method than feature-matching for the SLAM algorithm is to locate its positioning is scan-matching. Feature-matching refers to calculating absolute positioning while scan-matching refers to calculating relative positioning. The main difference is that in feature-matching the features are matched and in scan-matching, the scan points are matched [36]. The matching can be executed with many known algorithms such as Iterative Closest Point (ICP), Iterative Closest Line (ICL), Iterative Closest Plane (ICP), and Maximum Likelihood Estimation [40].

The drift can be caused by many factors such as misalignment of the start and stop location (loop closure), movement of objects in the environment, nonoptimal measurement path within the environment and the elapsed time in the data collection [16,18,41]. The start and stop locations of the closed SLAM laser scanning measurement are recommended to be the same. Otherwise, it can lead to their misalignment [41]. Movement in the environment can be as minimal as opening and closing doors or passing vehicles. However, these can lead to drift as recognized in the studies by Raval et al. [16] and Keitaanniemi et al. [18]. In addition, the path of the SLAM laser scanner affects the errors of the resulting point cloud. SLAM algorithms use the iterative alignment of detected features to locate themselves in the environment. For this reason, closing loops are preferred in SLAM laser scanning to cope with dynamic drifting. Sometimes in nonideal cases, the measurement path does not provide the required number of features for the SLAM algorithm to function reliably, which leads to drifts in the path solution and thus distortions in the point cloud [18,41].

## 3. Materials and methods

### 3.1. Case study

#### 3.1.1. Study site

To examine the behavior of the drift of SLAM point clouds and the effect of post-processing, we collected point clouds at an Aalto University Campus in Espoo, Finland. We selected a four-story 1960s university building for our study site. It was designed by the architects Jaakko Kontio and Kalle Räike. The building has the typical features of a campus building such as lecture and meeting rooms and corridor environments [42]. The study site is in Fig. 2a and it includes the hallways of the two first floors of the campus building, four rooms, and a small section in front of the building (Fig. 2b). Overall, the study site is circa 950 m<sup>2</sup>. All rooms and hallways are furnished with tables and couches and thus the SLAM algorithm has features to use for locating itself. There are six stairways in the study site which are the most featureless and narrow environments for SLAM with a narrow corridor on the first floor. In addition, the entry has many glass windows and walls, as does the 2nd floors hallway in front of the two smaller meeting rooms. In all the other locations there are many features close to the sensor. The study site also included a small section in front of the building that has a number of the features for SLAM. However, these features were only next to the building because of the wide street and the grass area next to the building (Fig. 2b).

#### 3.1.2. Datasets

The reference point cloud was collected with a Leica RTC360 terrestrial laser scanner with 63 scans and 24 target spheres. The measurements took three and a half hours. The scanning settings were 6 mm in resolution at a 10 m distance. The data were processed in Leica

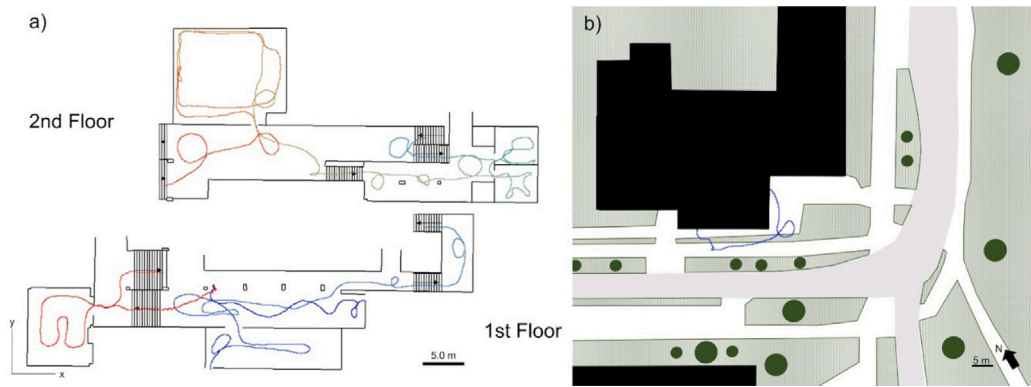


Fig. 2. Representation of the study site with the trajectory of the SLAM sensor colored from red to blue as start to finish. (a) Floorplan of the study area inside the building (b) Area outside the building has green grass areas with some trees (circles), street (gray), and sidewalks (white).

Cyclone Register 360 software with a combination of cloud to cloud and target-based alignment resulting in an absolute mean error of 3 mm.

The SLAM point cloud was collected with a GeoSLAM ZEB-REVO laser scanner with a range of 30 m, a rotation speed of 0.5 Hz, a scanner profile frequency of 100 Hz, and a data acquisition rate is 43,200 points/sec. The vertical field of view is 360°, and the horizontal is 270° [43]. It was executed as one scan in ten minutes with slow walking speed. In addition, during the walking path, we created internal closed loops in the rooms and hallways, as shown in Fig. 2. The data was processed in GeoSLAM Hub software with default settings.

### 3.1.3. The SLAM algorithm of the ZEB-REVO

The algorithm of the SLAM laser scanner estimates trajectory and sensor translations and rotations during the scanning. As new data is acquired, the algorithm uses the time window of the trajectory to process that data with information from the previous time step. Each segment of the data is processed iteratively. During the iteration, the algorithm identifies the corresponding surface patches from the point cloud. The second step of the iteration updates the trajectory. This step minimizes errors between matched surfaces and deviation from the measured inertial measurement unit's (IMU) accelerations and rotational velocities. It also estimates time synchronization and IMU biases [44].

After the iterative SLAM algorithm phases, the algorithm executes global registration. For it, the algorithm requires an initial parameter of the trajectory from the IMU. This trajectory should be a closed loop. In this phase the algorithm processes the entire trajectory as one window. The rest of the iteration steps are the same as in the case of segmented windows [44].

## 3.2. Analysis of the post-processing improvements

To demonstrate the behavior of the drift in the SLAM point cloud we compared the drifted SLAM point cloud to the reference point cloud. This process is described in more detail in Section 3.2.1. In addition, we post-processed the SLAM point cloud with two different SLAM point cloud section sizes and with two different correction algorithms. To analyze the discontinuity of the SLAM point cloud after sectional post-processing we compared the statistical values of the overlapping area between the SLAM point cloud sections.

### 3.2.1. Initial situation analysis

To illustrate the drift in the dataset we aligned the SLAM point cloud to the same coordinate system as the reference point cloud using CloudCompare. This was executed using ICP (iterative closest point) calculation. For the ICP calculation, the SLAM point cloud was segmented to include only points from the first 99 s. In addition, the reference was manually segmented to cover the same area. These

Table 1

Steps of the classification macro used in Terrascan with definitions.

Name of the step	Definition
ScanCutLong	Cuts off long range measurements from the features that are detected multiple times with the sensor
ScanClassifyRange	Classified all the points that are over 15 m from the scanner
ScanClassifyIsolated	Removes isolated points that had only one two neighbors within 0.2 m radius
ScanClassifySurface	Classified points to a surface with 0.015 m tolerance
ScanSmoothenXyz	3D smoothing process based on the 25–30 neighboring points by fitting 2nd degree surface to the points
ScanThinGrid3d	Removes some of the points that are within a grid cell which is 0.2 m in size

segmented point clouds were aligned with ICP. The rest of the SLAM point cloud was transformed to the same coordinates as the first 99 s with the transformation matrix of the ICP calculation. With this process, we obtain at least the beginning of the drifted SLAM point cloud to align with the reference. After alignment, we removed the noise of the SLAM point cloud with a classification macro in Terrascan (Terrasolid, Finland). The macro classified points that are over the sensor's range, lonely clusters of points, and points from plane surfaces that were over a threshold from the median value. The steps of the classification macro are explained in more detail in Table 1 [45]. Then these classes were removed before rest of the processes.

After alignment and noise removal, the SLAM point cloud was manually segmented into eight sections which were 52–119 s in CloudCompare. Section lengths were chosen by the number of features in the section and based on the time of the detection of the points. From each section, we chose and segmented three planar surfaces with different orientations like a floor or a wall and calculated the distance difference between the SLAM point cloud and the reference point cloud. This was executed with the M3C2 plugin [46], implemented in CloudCompare. The plugin uses an existing point normal to create cylinders in a reference point cloud. These cylinders are then used for finding the intersections of the compared point clouds and the distance differences between them [46]. From the distance differences, we calculated the statistical mean and standard deviation by using Gaussian fitting in CloudCompare. These values indicate the accuracy before the further drift-removing post-processing in third-party software. The process is presented in Fig. 3.

To identify the drift error accumulation, we analyzed the SLAM condition data calculated in GeoSLAM Hub software. The data shows

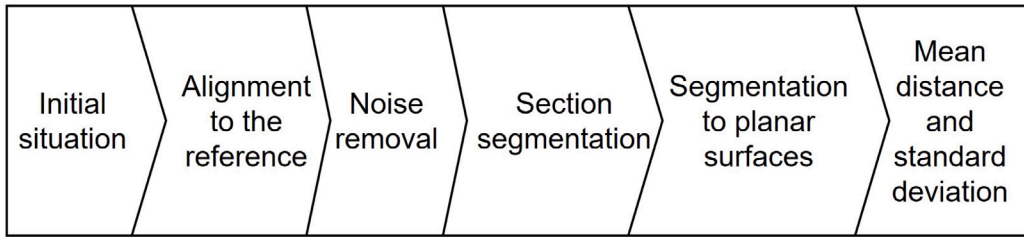


Fig. 3. Used process of demonstrating the drift error behavior in the initial situation.

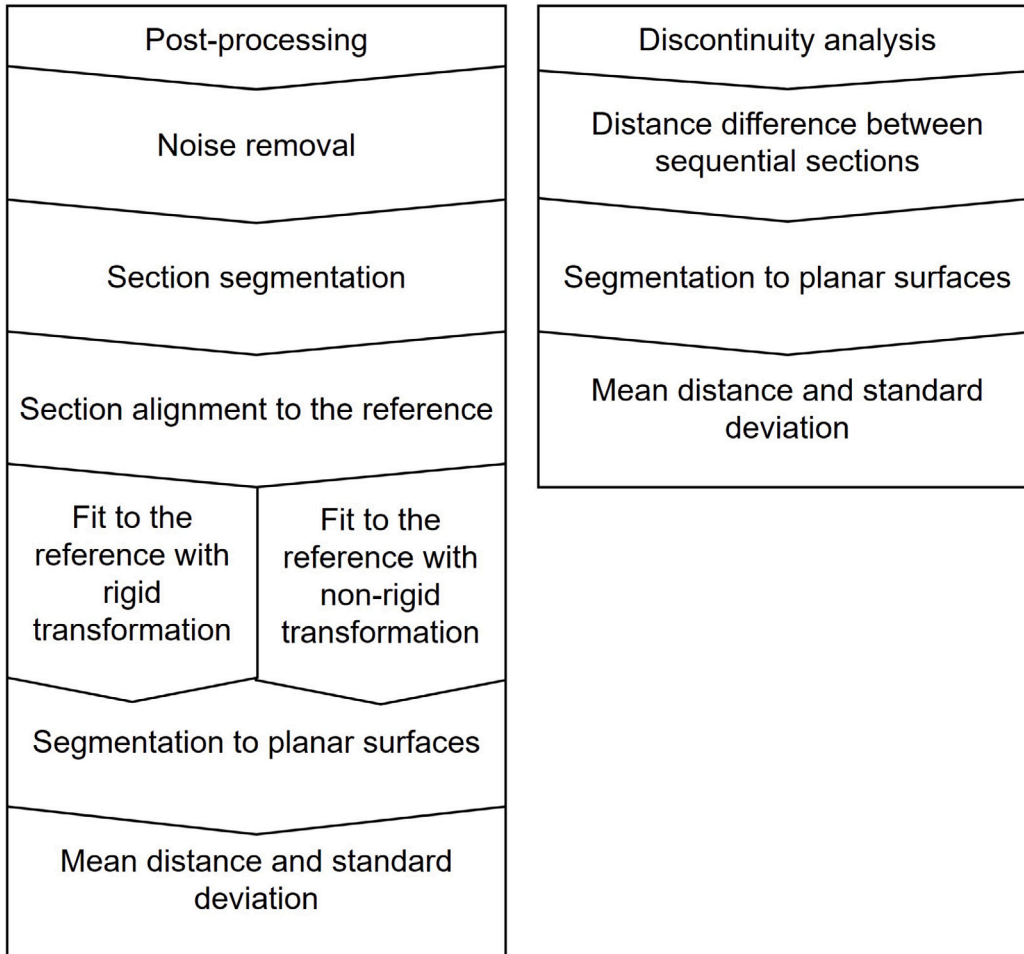


Fig. 4. Utilized post-processing process and the process to identify the discontinuity. The process was repeated at first with the large sections and then with the small sections.

how well the SLAM algorithm can use detected features. This data colors the SLAM point cloud from blue, a good SLAM value, to a red, a poor SLAM value [47]. The SLAM condition data was segmented in the same sections with the same method as before. For the analysis, we manually segment the points with poor SLAM value points in each section and visually analyze them based on the timestamps of the points and the trajectory.

3.2.2. Post-processing process

The SLAM laser scanner point clouds were post-processed in Terrascan (Terrasolid, Finland). At first, we aligned the SLAM point cloud sections to the reference point cloud with ICP in CloudCompare to give a mutual location to the sections before more detailed processing in

Terrascan. Then we removed noise from the SLAM point cloud sections with the same classification macro as in Table 1 in Terrascan. The detailed processing of the SLAM point cloud sections was executed with fit to reference with correction algorithms.

Before post-processing in Terrascan, we created a reference point cloud that included 6–10 small, manually segmented areas of the reference point cloud. These segmented parts included 30 × 30–60 × 60 cm planes or segments of the furniture or other structure in the environment. The same areas that were segmented to be the reference point cloud for the post-processing were manually classified as one class in the SLAM point cloud sections in Terrascan. In the post-processing, the fit to reference with correction algorithms was executed only based on the segmented reference areas and the manually classified SLAM

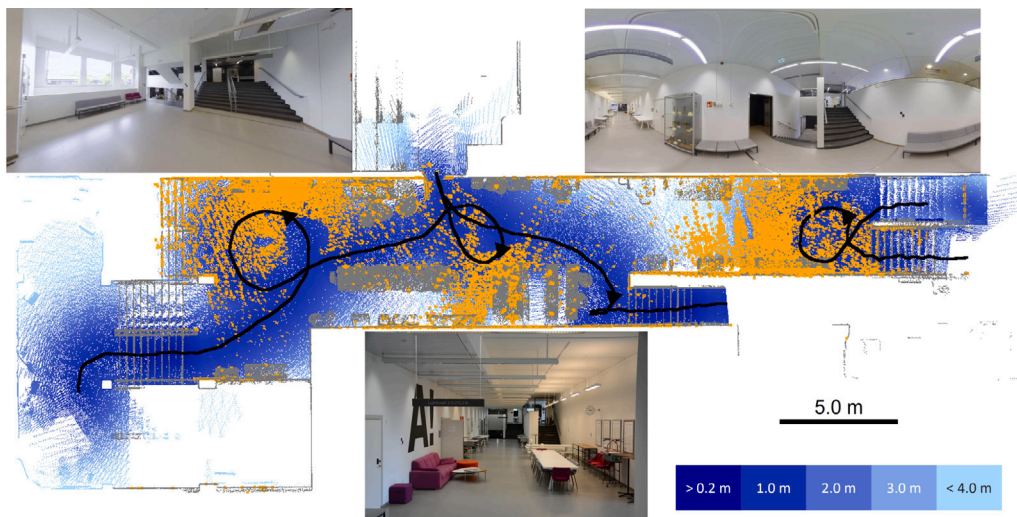


Fig. 5. Illustration of the poor SLAM value points in the internal loops of the walking path on the second floor. All the detected points of the hallway are represented with blue colors based on the distance to the walking path (black). The hallway features are colored gray, and the poor SLAM values are represented with orange. The starting locations of the poor SLAM value detections are marked with black triangles in the walking path. In addition, the hallway images represent the environment in the internal loop locations.

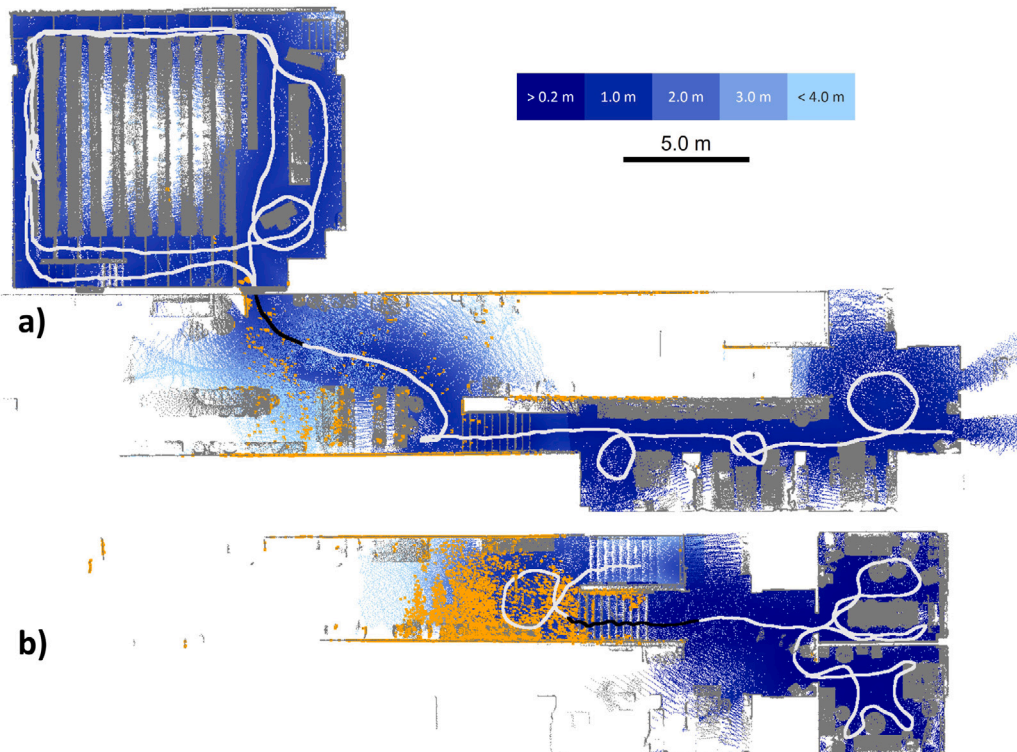


Fig. 6. Representation of the poor SLAM valued transitions in sections 3–4 and 5–6. All the detected points of the environments are represented with blue colors based on the distance to the walking path. The features of the environments are colored gray, and the poor SLAM values are represented with orange. The walking path is colored black in the areas that have detected poor SLAM values and white in the rest of the sections. (a) narrow doorway in sections 3–4 (b) narrow staircase in sections 5–6.

points. For the correction algorithms, we concentrate on the data-driven methods of drift error reduction. There are several correction algorithms of the data-driven method. However, we concentrate on rigid and non-rigid transformation algorithms. The rigid transformation includes only translations and rotations of the point cloud. In contrast, the non-rigid transformation, also known as an affine transformation, includes deformations besides translations and rotations [48]. Both of these correction algorithms are implanted to the SLAM point cloud in the post-processing phase with manually segmented reference points that are used as control points. The correction algorithm was executed in fit to reference by choosing different settings in the method. In the

rigid transformation, the correction was applied systematically using transitions in XYZ directions and rotations around the XYZ axes based on the earlier defined reference point clouds. The non-rigid transformation differs only with the setting that allows deformation in the correction. The deformation is executed with a correction model based on the correction vector. The algorithm calculates the correction vector based on the reference point clouds and interpolates the values between the reference point clouds [45].

As in the initial situation, we chose and segmented the same three planar surfaces from each section and calculated the distance difference between the SLAM point cloud and the reference point cloud with the

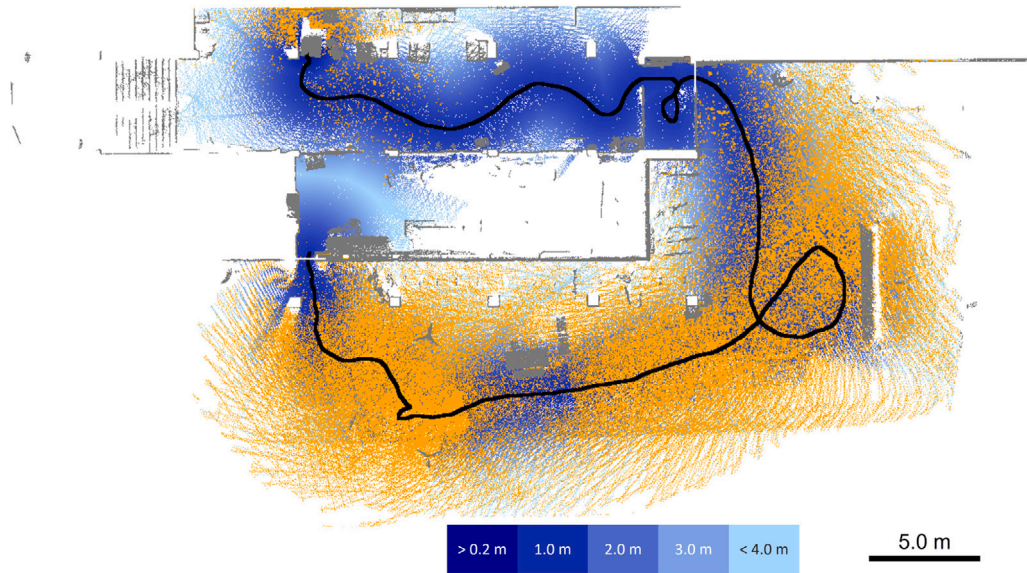


Fig. 7. Distribution of the poor SLAM value points detected in section 8. All the detected points of the section are represented with blue colors based on the distance to the walking path (black). The section features are colored gray, and the poor SLAM values are represented with orange. The white lines represent the doorways, and the outside area is measured with the trajectory that is between them.

M3C2 plugin. In addition, as in the initial situation, we calculated the statistical mean distances and standard deviations by using Gaussian fitting and the average value of mean distance and standard deviation from all the section values. The processing process is shown in Fig. 4.

In addition, we analyzed the discontinuity of the sections after the post-processing in CloudCompare. We calculated the distance difference between sequential sections of the SLAM point cloud with the M3C2 plugin. From the distance difference calculations, we segmented three planar surfaces from each overlap area and calculated the mean distance and the standard deviation with Gaussian fitting.

Based on the results of the first sections of the SLAM point cloud we tested the same process with smaller sections that were from a 31–37 s timespan. The larger sections were divided into smaller ones only in the middle of the measurement path (270–475 s). The largest difference in the mean distance values was detected between those sections. The rest of the processing steps were executed in the same way as with the larger sections. We then compared the mean distance and standard deviation results of the sections and the discontinuity of the sections.

## 4. Results

### 4.1. Analysis of the SLAM point cloud values during the walking path

The SLAM point cloud values based on the SLAM condition calculation of the GeoSLAM Hub are shown in Figs. 5–7.

### 4.2. Analysis of the large sections

The SLAM point cloud was aligned to the reference point cloud based on the first 99 s of the measurement path. That part aligned to the reference with a root mean square error (RMSE) of 0.9 cm and the rest of the measurement path was transformed to its location based on the transformation matrix of that first section. The reference was aligned with this method because we knew that the SLAM point cloud had drifted and the probability that the drift had happened after the first 99 s was high based on the environment. The results of SLAM point cloud section alignments to the reference before post-processing are presented in Table 2 with information of the sections. The sections

Table 2

Display of the used section names, timestamps of the sections, lengths of the trajectories inside sections, and the number of the points in the sections. In addition, there are the root mean square errors (RMSE) of sections from alignment to the reference before post-processing.

Large sections				
Section names	Section timestamp seconds (s)	Length of the trajectory in section (m)	Amount of points in section (pcs)	RMSE (cm)
Section 1	0–99	46	2990203	0.9
Section 2	99–151	37	1720713	1.0
Section 3	151–270	87	3799419	1.4
Section 4	270–337	46	2134908	1.4
Section 5	337–410	41	2388159	1.4
Section 6	410–475	46	2161973	1.4
Section 7	475–553	69	2272136	1.0
Section 8	553–654	68	318001	1.2
Small sections				
Section name	Section timestamp seconds (s)	Length of the trajectory in section (m)	Amount of points in section (pcs)	RMSE (cm)
Section 4.1	270–305	24	1102939	1.1
Section 4.2	305–337	22	1031969	1.3
Section 5.1	337–373	20	1277863	1.4
Section 5.2	373–410	21	1110296	1.5
Section 6.1	410–444	24	1045176	1.3
Section 6.2	444–475	22	1116797	1.1

are illustrated in Fig. 8. In addition to the timestamps, we measured the length of the trajectory which was circa 440 m, and the middle point of it was under section 4 timestamps. The average point density from five meters from the sensor is circa 1900–3300 points per square meter.

The mean distances and standard deviation values between the SLAM point cloud and the reference point cloud of the horizontal planes for the larger sections are presented in Figs. 9 and 10.

The mean distances and standard deviation values between the SLAM point cloud and the reference point cloud of the vertical planes for the larger sections are summarized in Figs. 11 and 12.

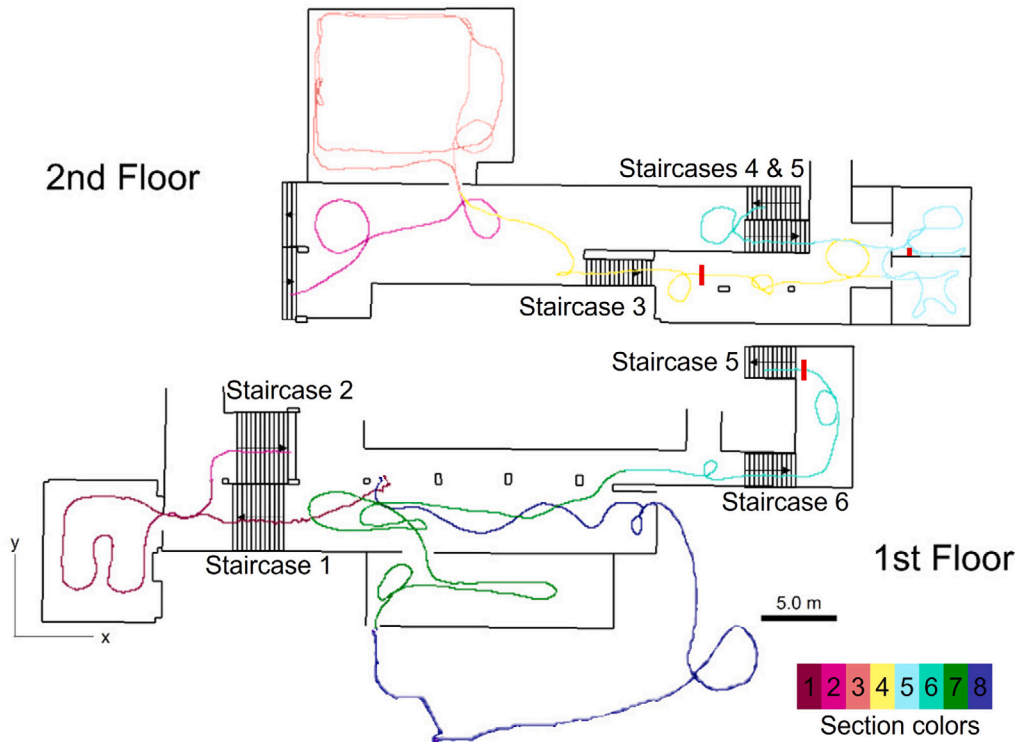


Fig. 8. Illustration of the sections in the floorplan of the study site. The large sections are represented with colors and the red lines represent locations that separate the smaller sections inside the large sections. The staircases are named with a number for analysis purposes.

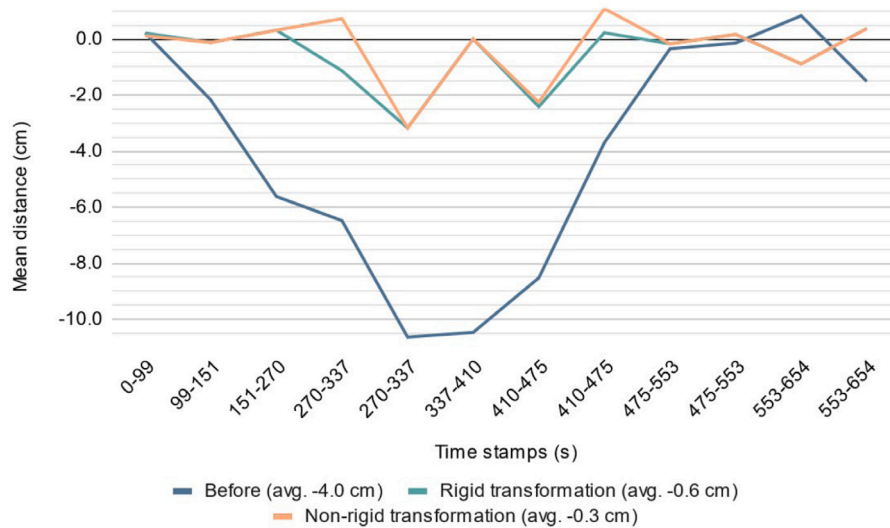


Fig. 9. Representation of mean distance of the horizontal planes between the SLAM point cloud and the reference point cloud in the large sections.

#### 4.3. Discontinuity of the sections

The mean distances of overlapping areas between consecutive large sections are shown in Fig. 13 for both correction algorithms. Correspondingly, the standard deviation values of overlapping section areas are shown in Fig. 14.

The mean distances of overlapping areas between consecutive small sections are in Fig. 15 with both correction algorithms. Correspondingly, the standard deviation values of overlapping section areas are shown in Fig. 16.

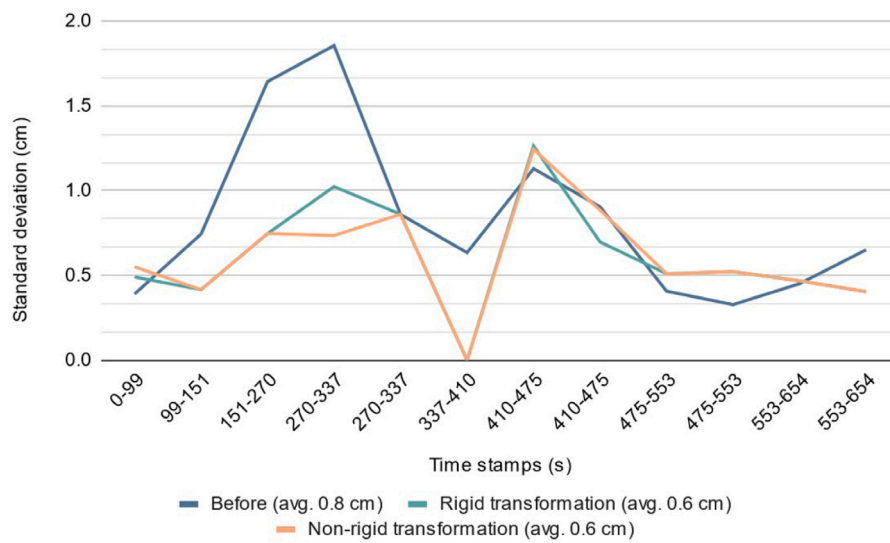


Fig. 10. Representation of standard deviation of the horizontal planes between the SLAM point cloud and the reference point cloud in the large sections.

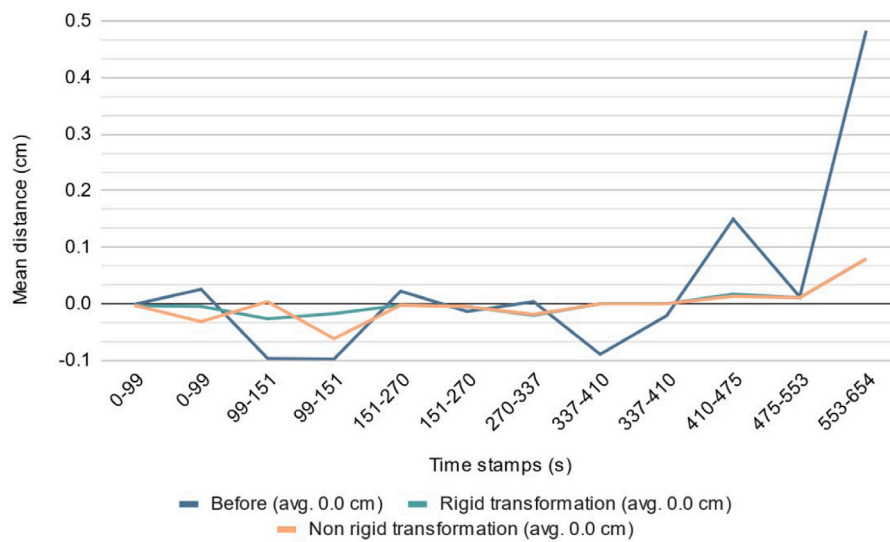


Fig. 11. Representation of mean distance of the vertical planes between the SLAM point cloud and the reference point cloud in the large sections.

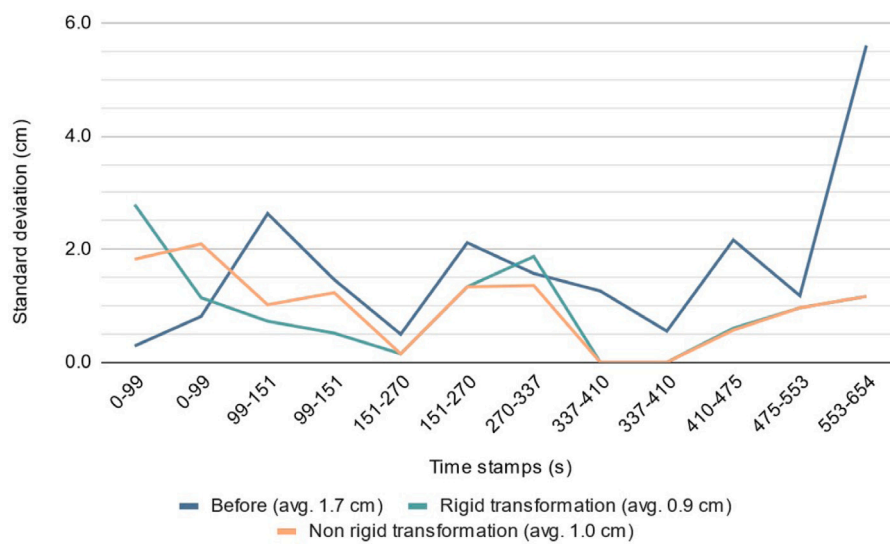


Fig. 12. Representation of standard deviation of the vertical planes between the SLAM point cloud and the reference point cloud in the large sections.

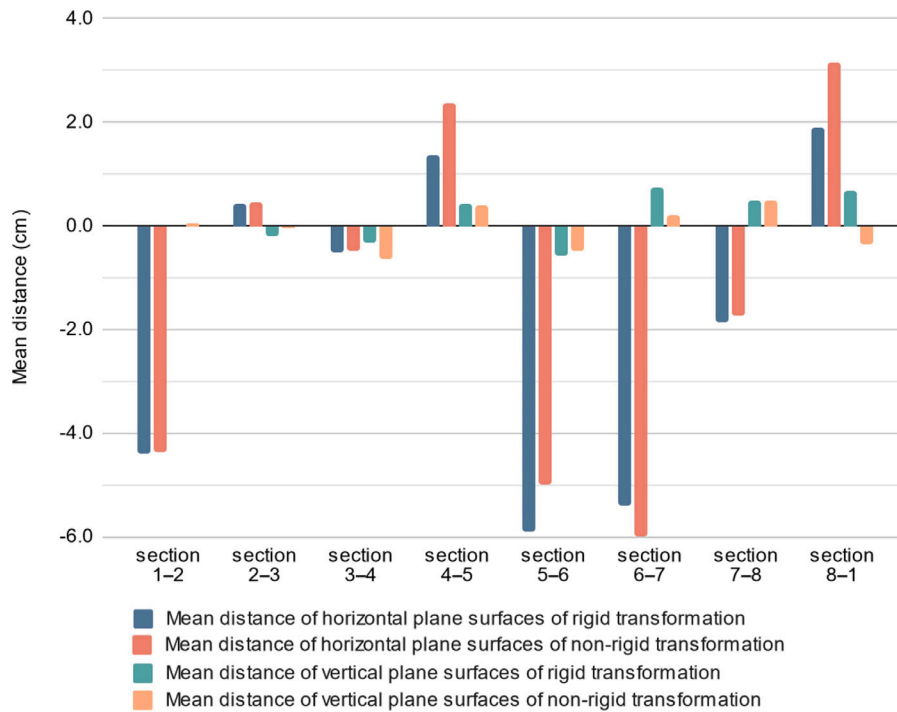


Fig. 13. Mean distances of overlapping areas of consecutive large sections are represented in rigid and non-rigid transformation.

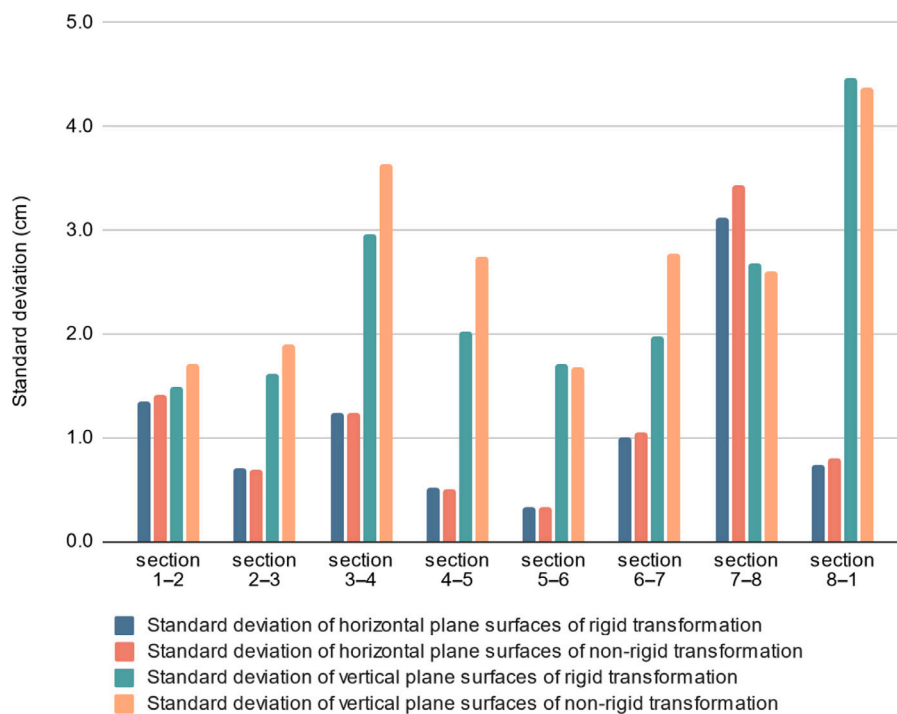


Fig. 14. Standard deviations of overlapping areas of consecutive large sections are represented in rigid and non-rigid transformation.

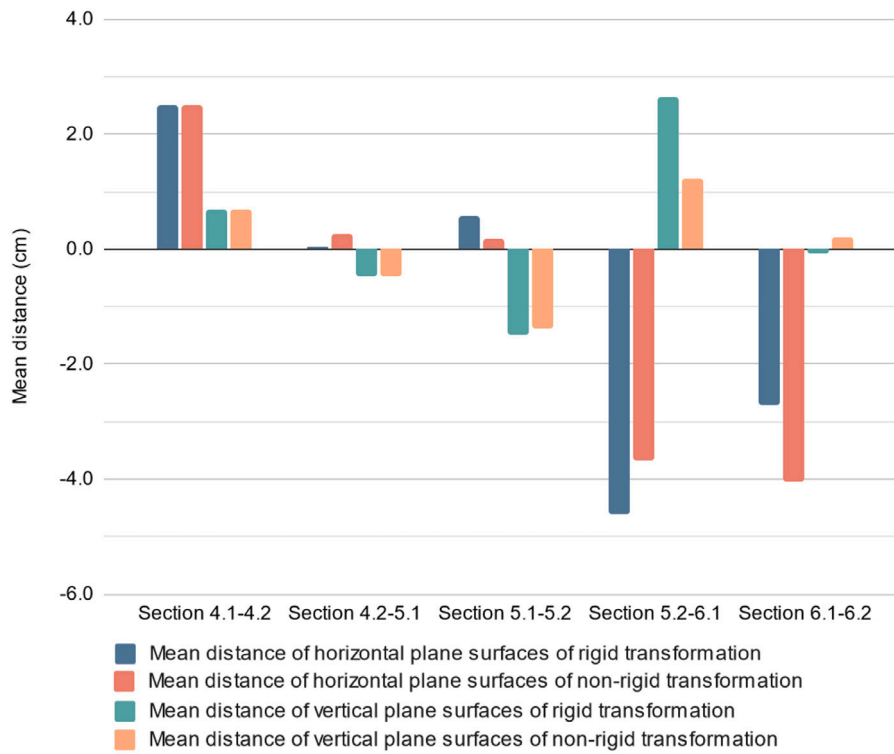


Fig. 15. Mean distances of overlapping areas of consecutive small sections are represented in rigid and non-rigid transformation.

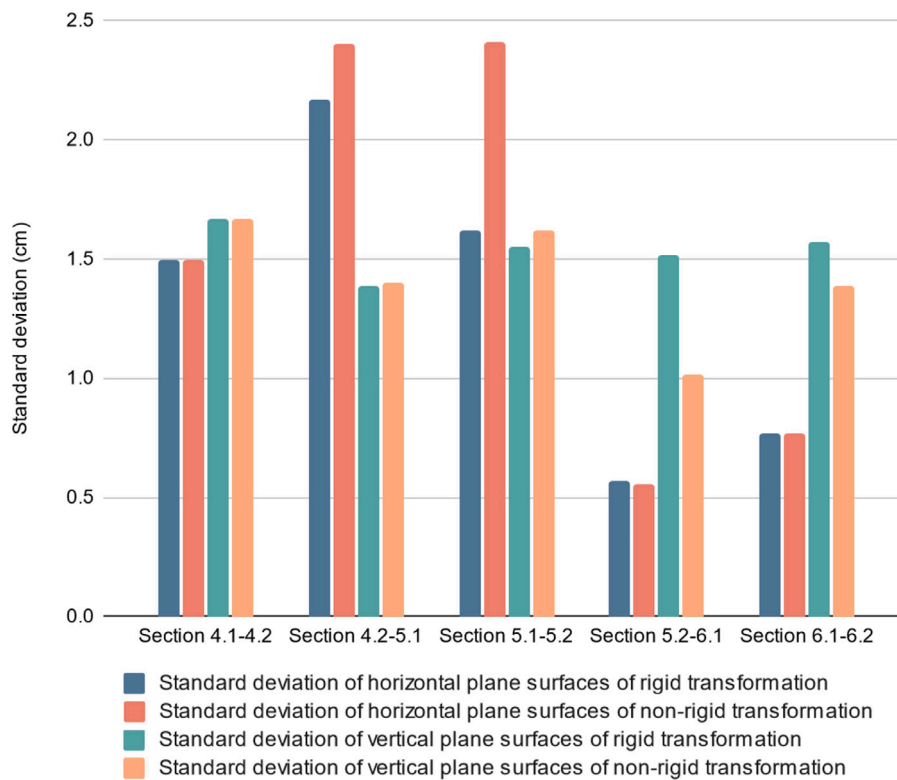


Fig. 16. Standard deviations of overlapping areas of consecutive small sections are represented in rigid and non-rigid transformation.

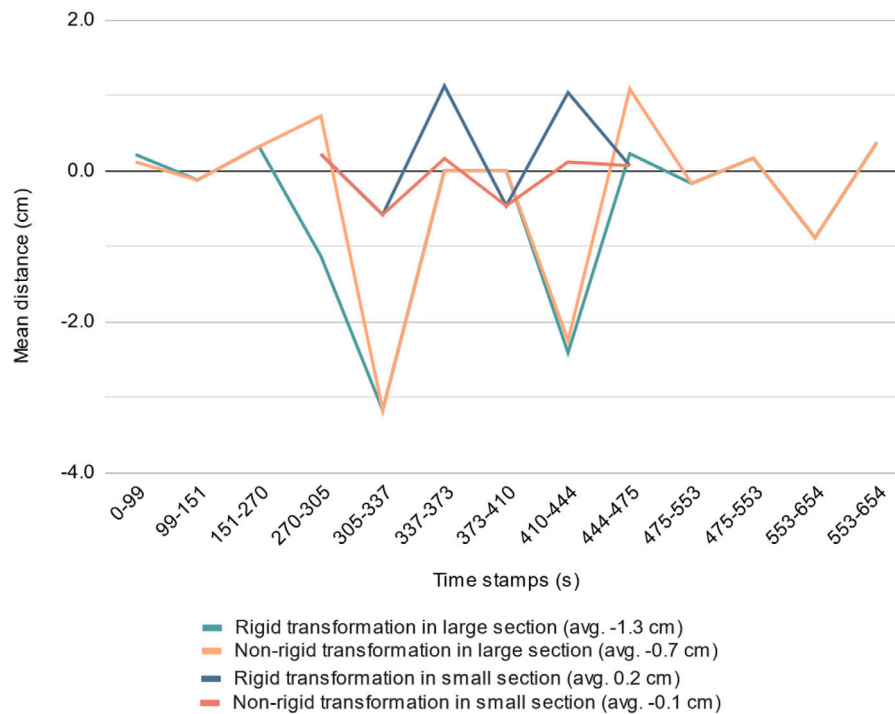


Fig. 17. Mean distance of the horizontal planes is presented between the SLAM point cloud and the reference point cloud in the large sections and small sections of rigid and non-rigid transformations.

Table 3

Average results of the discontinuity analysis with mean distances and standard deviations of the horizontal and vertical planes from overlapping areas between consecutive sections.

	Rigid transformation of large section (cm)	Non-rigid transformation of large section (cm)	Rigid transformation of small section (cm)	Non-rigid transformation of small section (cm)
Average of mean distances of vertical plane surfaces	0.2	-0.1	0.3	0.1
Average of mean distances of horizontal plane surfaces	-1.8	-1.5	-0.8	-1.0
Average of standard deviations of vertical plane surfaces	2.4	2.7	1.5	1.4
Average of standard deviations of horizontal plane surfaces	1.1	1.2	1.3	1.5

#### 4.4. Comparison of the large and small sections

The mean distance values between the SLAM point cloud and the reference point cloud of the larger and smaller sections of rigid and non-rigid transformations are shown in Fig. 17 in the horizontal direction and Fig. 19 in the vertical direction. The standard deviation values of rigid and non-rigid transformations are shown in Figs. 18 and 20.

The average values of the discontinuity analysis from overlapping areas between consecutive sections are shown in Table 3.

## 5. Discussion

### 5.1. Error behavior in the drifted SLAM point cloud

Based on the first results of the alignment of the SLAM point cloud to the reference point cloud, it was clear that the SLAM point cloud had drifted in the vertical direction (Fig. 9). With further analysis of the initial situation, the hypothesis of drift being largest in the furthest distance from the start and end location is correct. The drift error of the horizontal planes of the original SLAM point cloud increases towards

the middle point of the measurement path and decreases towards the endpoint. The maximum drift error was 10.6 cm in the horizontal direction and it was inside section 4 (timestamps 270–337 s) that includes the middle point of the trajectory based on time and distance. The explanation for the largest drift value in the furthest distance is that the drift error is congested over time. Because of the close-loop measurement and the SLAM algorithm that tries to fit the start and end point together as well as possible, the drift moves away from that point and is congested to the furthest point of the measurement path. The congestion of the drift error could be avoided with additional control points during the measurement path which would be used in the post-processing to reduce the drift.

#### 5.1.1. Drift error locations

The drift error was analyzed according to the observations of measuring environment and walking path. Environments such as narrow doorways, narrow hallways with internal loops in the walking path, outside environments, and narrow staircases with a few features have led the SLAM algorithm to have decreased detection of the features to use in a SLAM algorithm. The drift error appearance locations and

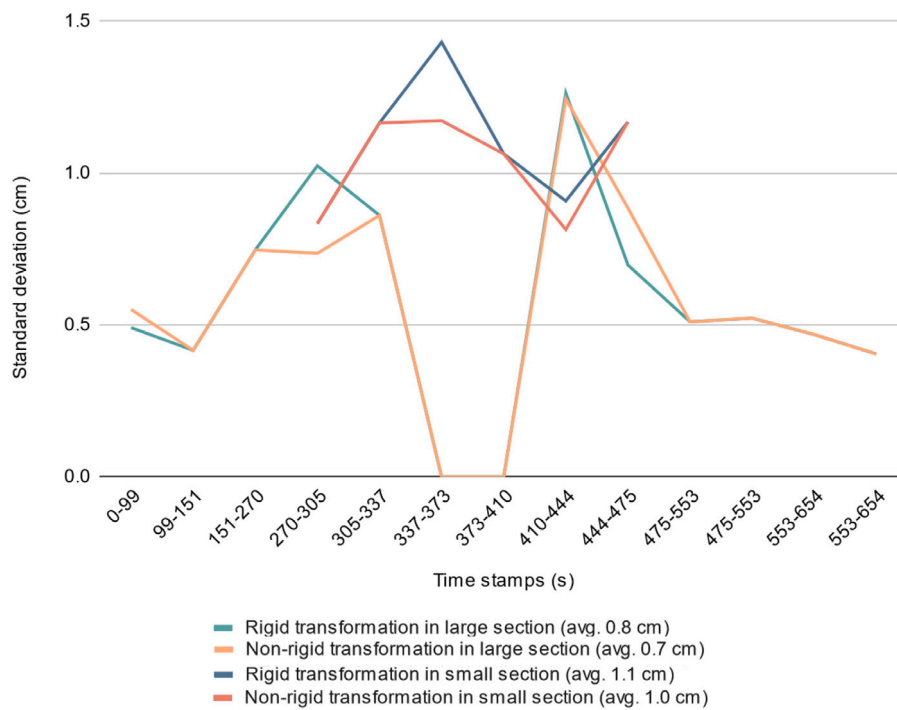


Fig. 18. Standard deviation of the horizontal planes is presented between the SLAM point cloud and the reference point cloud in the large sections and small sections of rigid and non-rigid transformations.

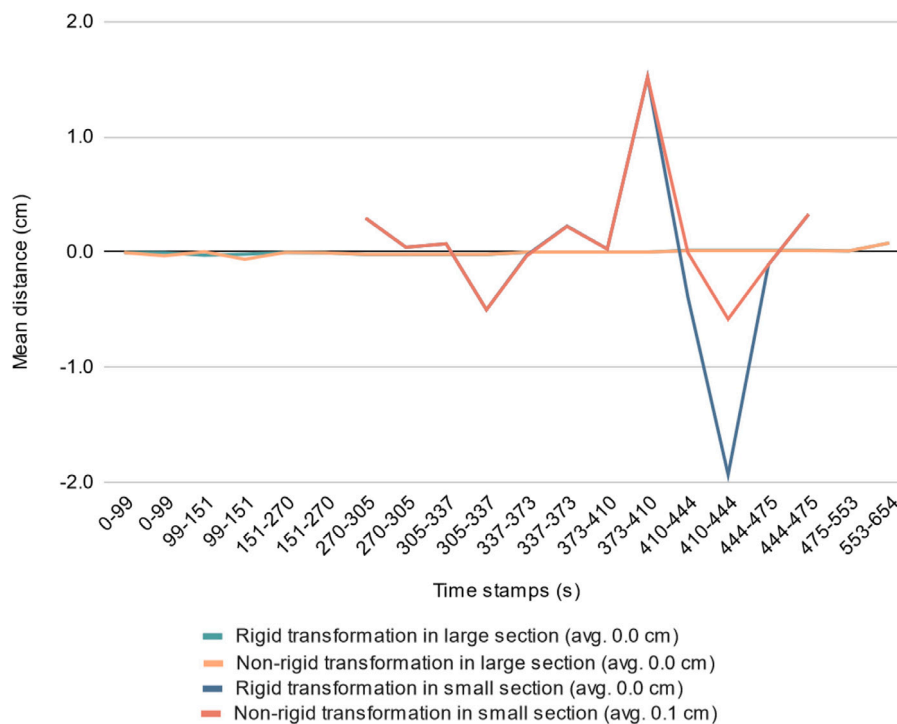


Fig. 19. Mean distance of the vertical planes is presented between the SLAM point cloud and the reference point cloud in the large sections and small sections of rigid and non-rigid transformations.

walking path characteristics to prevent it are listed in Table 4. The errors of the point cloud can occur in the narrow hallway during internal loops in the walking path (Fig. 5). The second-floor hallway is long and narrow (Fig. 8). The widest part of the hallway is 8.5 m

wide, and the narrowest part is 4 m wide. Most of the hallway is 6.5 m wide and 29 m long. In section 2, the trajectory has two internal loops. During these loops, the detected features had changed to the poor values for the SLAM. The first internal loop in section 2 starts to have

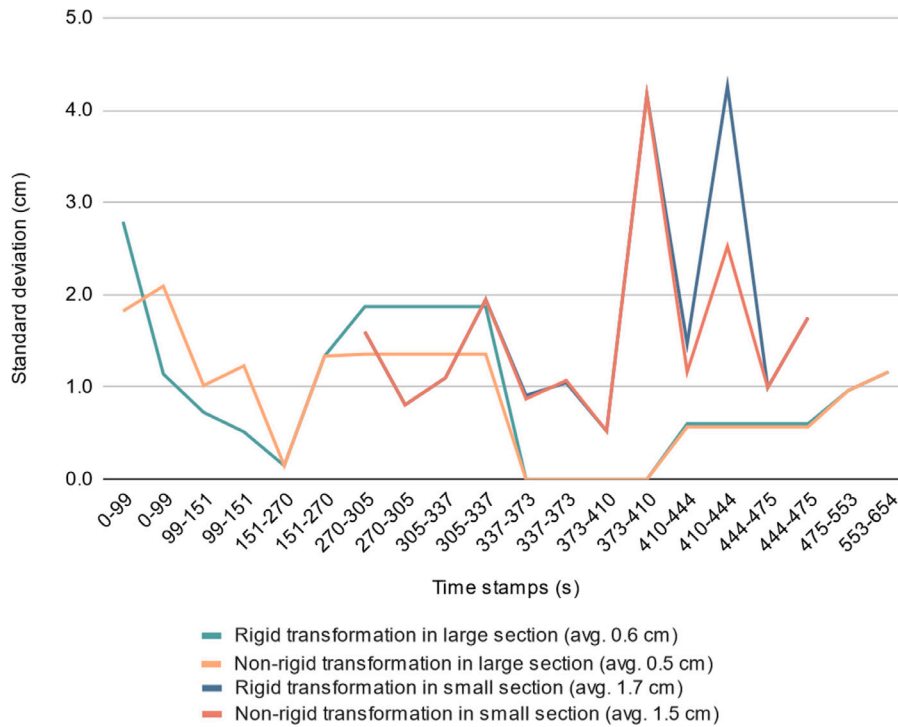


Fig. 20. Standard deviation of the vertical planes is presented between the SLAM point cloud and the reference point cloud in the large sections and small sections of rigid and non-rigid transformations.

Table 4

Illustration of drift error locations during the walking path increases the drift with a threshold value of 2 cm. In addition, the walking path characteristics have prevented or minimized the drift error during the walking path.

Section name	Locations that increase the drift with over 2 cm	Locations that increase the drift with under 2 cm	Drift preventing walking path characteristics
Section 1		Start of the SLAM measurement	Walking path under 10 m from features and internal loop around furniture
Section 2	Small internal loops in the second-floor hallway that is long and narrow		Straight walking through the long and narrow hallway with features under 10 m
Section 3	Small effect of the narrow doorway. However, it mainly accumulated from section 2		Several internal loops around the room's edges
Section 4	180-degree turn before staircase 3 and error accumulation of the previous drift locations	The narrow doorway causes a slight drift increase	The narrow doorway causes a slight drift increase
Section 5		Beginning of the transition to the staircase 4	Internal loops in circa 20 square meter rooms
Section 6	Internal loop in the second-floor hallway	After the transition of the staircase 4	Internal loops in smaller hallways between the staircases
Section 7	Accumulation of the drifts from sections 6 and 8		Internal loops with under 10 m from features and revisiting the measured environment
Section 8	Outdoor visit and end of the SLAM measurement		Revisiting the measured environment

poor SLAM values while turning toward the stairs next to staircase 2 (Fig. 5). Most of the already detected features stay under the gap in the sensor's field of view (FOV) during the internal loop. The other features are self-repeating staircases or features with over 5 m distance from the sensor. The direction of the internal loop towards anti-clockwise may have caused the poor SLAM values because most of the features are in the middle of the hallway.

The second internal loop in section 2 has poor values of the features after turning toward the width direction of the hallway (Fig. 5). The gap in the FOV covers some of the earlier detected features. The features

on the sides of the sensor are over 10 m in the distance. The poor SLAM values may be caused by the internal loop's small diameter (circa 2 m). The small diameter leads to quick turns for the sensor, and the scanner profile frequency cannot collect sufficient data for the SLAM algorithm. The size of the internal loop requires to be scaled based on the size of the space. In smaller spaces, the same errors did not occur. The distribution of the features in a narrow hallway with a small diameter internal loop causes problems for the SLAM algorithm. The internal loop in section 6 near staircase 4 in the second-floor hallway has the same problems as the second internal loop in section 2. Some

of the features are close, but others are over 10 m in the distance, and the diameter of the internal loop is circa 2 m. In this case, the hallway is even narrower than in section 2. In section 6, it would have been better to create the loop as an ellipsoid towards the wider part of the hallway, while the walking path would have covered the same features again than in sections 2–4. In section 4, the 180° turn in the trajectory before staircase 3, has poor SLAM values. The poor values are smaller than section 2 in the first internal loop. This may be because the turn is executed towards the middle of the hallway. However, the turn is tight, which can cause poor SLAM values of the features.

In addition to internal loops in narrow hallways, a narrow doorway impacted the SLAM algorithm and the amount of drift (Fig. 6). In section 3, the drift is 3 cm larger after the narrow doorway. The narrow visibility of the features for the SLAM in transition through the doorway can cause the drift. The space after the doorway has only minimal detection of the features before the transition through the doorway. These detected features were insufficient to keep the SLAM localization errorless because they had poor SLAM values. The same effect was in section 4 with the same doorway. However, it was smaller because the drift error differs only circa 1 cm. This may be due to the SLAM algorithm already gathering information from both sides of the narrow doorway. The reason for the existing information is that the measurement path is revisiting the same space after the room behind the narrow doorway. For that reason, the SLAM localization works better, and the drift increases only a little bit. However, the features detected straight after the doorway from over 4 m distance had poor SLAM values.

Similarly that the narrow doorway impacted the drift the narrow staircase 4 in the transition between sections 5 and 6 (Fig. 8) impacted the drift. The drift changes circa 2 cm larger after the transition to the downstairs in the narrow staircase (Fig. 6). The poor SLAM values may be caused by the narrow hallway of the second floor and the half-glass walls on the stairs and upstairs. The upstairs features are in the blind spot because of the narrow staircase and the gap in the sensor's FOV. Tilting the sensor more perpendicularly to the stairs would have avoided this. By tilting the sensor, the blind spot of the FOV would be covering a more featureless part of the environment.

Section 8 has a small (circa 0.7 cm) drift change in the horizontal planes after a brief visit outside. It is detectable in the SLAM values of the features, which are primarily poor on the outside (Fig. 7). Some of the poor SLAM value detections are right before the end of the measurement during the sensor's placement on the table. The same phenomenon is detectable at the start of the measurement. The poor SLAM values after the start have a minimal effect on the drift because the drift is 0.2 cm in section 1. The change in the feature distribution can cause the drift of section 8 outside. The wide street next to the building does not have many suitable features for the SLAM algorithm. For that reason, the features are mostly on one side of the sensor. Besides, indoors the floors, ceilings, and walls are all suitable for the SLAM algorithm to locate itself. In addition to them, the furniture and other objects add more diversity to the features, which helps the SLAM algorithm to do more precise locating. However, the coming back to the indoors in section 8 minimizes the drift in the section. Because the returning space is the same hallway as the starting and ending location, the drift is not accumulated in the poor SLAM value area. The processing of the SLAM point cloud has moved the error of the poor SLAM values further away from the end location, and they accumulate in the earlier sections (3–6).

The accumulation of the poor value errors changes the drift error to a different location than the poor SLAM values. The most significant accumulation of the drift error is in the furthest location (section 4) from the start and end location. From the start to the most distant location through section 1 to 4, the overall drift accumulation is 10.6 cm. A small part of the error of the internal loops in section 2 is shown in the drift between sections 1 and 2 (Fig. 8). The drift accumulates slightly between these sections. In section 3, the drift is circa 3 cm larger than

in section 2. This is due to the internal loops in section 2 and the narrow doorway in section 3. The largest effect of the error of the internal loops in section 2 has accumulated in section 3. In addition, the drift accumulates from section 3 to section 4 because of the narrow doorway. This accumulation between sections 3 and 4 on both sides of the narrow doorway may be small because the walking path goes through already detected features. However, the error accumulates circa 4 cm in section 4 after staircase 3. The reason is the 180° turn before the staircase and the other error areas that have been before section 4.

The same effect is from section 8 to section 4. In section 8, the drift occurs from the outside visit with a small accumulation. This may have the same effect as between section 3 and section 4 because section 8 returns to the same space as the whole measurement has been started. The return to the same room as the starting location is shown in the drift between sections 8 and 7 with a small accumulation. After staircase 6 in section 6, the drift has accumulated circa 3 cm more from section 7. The drift grows circa 4 cm in staircase 5. All this accumulation between sections 8 and 6 are caused by the outdoor visit and the internal loop in section 6. In section 5, the drift accumulates based on the narrow staircase 4. All the drift accumulates to sections 4 and 5 even though they had a minimal amount of the poor values of the features for the SLAM algorithm to solve itself. Walking path extension to cover the same features as in sections 2–4 of the narrow hallway on the second floor would have minimized the amount of the drift in section 6.

#### 5.1.2. Recommendations for the locations of the control points

Based on these results, the locations of the additional control points should be after narrow staircases that lead to the narrow but high ceiling hallways with a low number of features, in long and narrow hallways, near narrow doorways, and outside during transitions between inside and outside measurements. After narrow and almost featureless staircases should add control points. Significantly in transitions to narrow high ceiling hallways after the narrow stairs. In narrow featureless hallways, it is important to add a control point. Adding at least two control points before and after a narrow hall would be good. However, if it is over 30 m, adding a control point in the middle of the hallway is not a bad idea. Control points could be located on both sides in narrow doorways if the measurement path enters and exits from the same doorway. The control point should be located after a narrow doorway in other cases. It is important to have a control point outdoors while visiting there. Even though the outdoor environment does not have the same feature distribution as in this study, traffic or other types of movement may affect the SLAM algorithm.

These control points could be used to prevent drift either during the SLAM algorithm calculation or during post-processing on construction sites. In some of the SLAM laser scanners on the market, adding a control point for SLAM algorithm processing is possible. The results of this study indicates some of the places that require control points so that drift can be prevented in SLAM laser scanning. Based on this information, limiting the control points to only useful locations is possible. However, if the drift occurs despite the control points it is possible to use the same control points in the post-processing with third party software. Besides, it may need a couple of control points in possible error areas depending on the post-processing method. In addition, additional control points in problem areas may bring closer the possibility of creating automation in construction monitoring and quality controlling with SLAM laser scanners.

#### 5.2. Analysis of drift error reduction in post-processing

In addition to the error behavior, we studied error reduction with sectional post-processing. Overall, the post-processing reduced drift error in all directions with both section sizes. The maximum drift reduction was 10.4 cm. However, this was not the case with small sections in the vertical direction (Fig. 19). There the average mean distance

between the SLAM point cloud and the reference stayed at the same or increased some millimeters in the sections. In addition, the average of the standard deviations between the SLAM and reference point clouds decreased after post-processing with large sections (Figs. 10, 12, 18 and 20). With small sections, the same increase was detectable as in the mean distances. The reason for this may be that the noise removal used medians of the point cloud surfaces to reduce noise. It was executed before the transformation algorithms. With the smaller sections, the median could easily be in a different location by a couple of millimeters than with the larger sections based on the amount of the data.

The vertical planes have under a 0.5 cm mean distance from the reference point cloud before the post-processing of the SLAM point cloud (Fig. 11). This can be due to the sensor's accuracy which is 1–3 cm [49]. For the large sections the average mean distance does not change after post-processing. For the small sections (Fig. 19) the mean distance of the section increases over the values that were present before post-processing. This shows that it is not profitable to post-process the points from the direction that already has good values. Particularly, the average of the mean distance from all the small sections is almost the same as before post-process. These are as well under the sensor's accuracy. In conclusion, the drift is mainly detected only in one dimension. Because the drift is mainly in one dimension, in the future drifted SLAM point clouds could be processed in only the direction that has the drift. Based on the results, the differences between non-rigid and rigid transformations are relatively small. Overall, the difference is from a couple millimeters to a half of centimeter (Figs. 17–20). However, this is dependent on the case because it is possible to have drift in SLAM point clouds in many directions.

In the sectional post-processing, the continuity between the sections is important. Based on the average results of the discontinuity analysis the small sections have smaller changes between horizontal planes than the larger sections (Table 3). At the same time the change is almost the same for both section sizes in vertical planes. This is shown also in Fig. 13 which has four overlapping sections with over a 2 cm mean distance between sections and in Fig. 15 where the number of sections that are over 2 cm is three. In addition, the standard deviations are smaller in the small sections than in the large sections (Figs. 14 and 16).

The hypothesis of smaller sections reducing drift more than large sections was correct in the horizontal planes. With the small sections the average mean distance between the SLAM point cloud and the reference point cloud was close to 0 cm. At the same time the value for the large sections was 0.7 cm at the best. Because the results for the vertical planes were the same with both sections it does not affect the selection of the section size in sectional post-processing. In addition, small sections show better results in the discontinuity analysis between sections. The only downside with the small sections is that the standard deviation between the SLAM point cloud and the reference is on average 0.2–0.3 cm larger with the small sections than with large sections. For the transformation algorithms the section size has a small effect. With the small sections the non-rigid transformation is circa 0.6 cm better than with large sections and in rigid transformation the difference is circa 1.5 cm. In addition, the non-rigid transformation algorithm is better in horizontal plane errors and rigid transformation in vertical plane errors. Overall, the choice of the section size and post-processing algorithm is dependent on the application and needed accuracy. Smaller sections reduce drift more, however, larger sections also have results that fall below the sensor's accuracy.

Even though our post-processing gives promising results of reducing drift error, a method that requires collecting both a SLAM point cloud and some other more accurate point cloud such as a terrestrial laser scanner point cloud is not an optimal way to execute the post-processing of a SLAM point cloud. However, it proposes that sectional post-processing with the correction algorithms in third-party software is a possible method to reduce a noticed drift error in a SLAM point cloud. The other optional methods to reduce drift would be a tool

that reduces the error over time, such as an interpolation, time-based leveling, or time-based linear transformation [21,50–52]. However, the authors are not aware of any third-party software that includes any of these error reduction methods. However, sectional post-processing could also be executed by using added control points such as spherical targets for reference information in the post-processing. Some of the required and critical control point locations (as featureless staircases, narrow hallways and doorways) have been identified and discussed in this study. The sectional post-processing method presented in this study could be used for example for construction documentation, monitoring and quality analyzing purposes. To identify real change between new and old datasets, the datasets should include as few errors as possible. Because SLAM laser scanning is a walkable method to collect 3D data from a construction site, it would be a useful tool for construction monitoring and quality analyzing. Even though it has sometimes presented drift errors, as we explained in the introduction, this can be reduced as the experimental study illustrates. However, in the case that the reference points for the sectional post-processing are taken from earlier point clouds there needs to be points that are definitely from stable features. If the reference points are stable, the results that are shown in this experimental study can be reached with multi-time construction documentation datasets by using the sectional post-processing process. In addition, if we add features that are detectable with SLAM laser scanners in the critical locations, it is even possible to prevent drift from occurring.

## 6. Conclusions

This paper demonstrated the behavior and correction of drift in a SLAM point cloud. The study case shows that the drift error was the largest in the middle of the trajectory based on time and distance, with a value of 10.6 cm. The SLAM LS can drift over 10 cm within ten minutes of measurement. Environment affects the drift, such as narrow staircases, long narrow hallways, narrow doorways, and visits from inside to outside. It would be important to add control points after or inside these locations to prevent drift errors from occurring. In addition, the measurement path can be optimized to prevent drift. For example, the measurement path should revisit the environments that have been measured. Similarly, the internal loops, which are scaled based on the size of the environment and measured toward the middle of the room, can minimize the drift. The internal loop diameter can be circa 2 m when the space is circa 22 square meters. However, in 220 square meters, the 2 m diameter in the internal loop is too small. The drift was mainly detected only in the vertical direction because, in vertical planes, the mean distance from the SLAM point cloud to the reference was 0.5 cm. In addition, the standard deviation is under 2.6 cm, which is within the sensor accuracy specification.

Sectional post-processing could reduce drift by from 10.6 cm to 0.2 cm in this case study. However, the drift error is detected to appear only in the vertical direction so that the post-processing could be executed only in that direction. Based on the results of this study, the horizontal direction can still be within the sensor accuracy specification. The building interiors can be measured at the level of 1–3 cm accuracy when the SLAM point cloud is errorless and the noise is removed. Regarding section size, smaller sections reduce the drift error more than larger sections. In addition, non-rigid transformation reduces drift error more than rigid transformation. However, the choice of section size and post-processing algorithm is still dependent on the application and required accuracy because the results have minimal differences. Based on the results, it is possible to conceive a measurement path that can collect errorless point cloud data from building construction. With this kind of measurement path, commercial SLAM LSs are even more suitable for future construction applications such as documentation, monitoring, and quality analysis. In addition, the effectiveness of SLAM laser scanners in construction applications is still possible even with drifted point clouds. The commercial SLAM

LSs could be even more suitable for construction quality analysis with additional control points. With the control points in critical locations, the drift error can be prevented on the construction site. Most importantly, the results show that the drifted commercial SLAM LS point cloud could be part of construction documentation. The reason is that the drift is possible to minimize in post-processing and new repeated measurements to replace the drifted ones are unnecessary, and the project stays on schedule.

Several topics need to be addressed in future research. As this research suggested, the additional control points can be used to prevent drift error. However, the value of the effect should be studied with commercial SLAM LSs. In addition, this study presents a style of the internal loop with SLAM LS with a maximum measurement range of 30 m. The influence of the extended maximum range with internal loops should be studied within the different sizes of spaces. As the paper presents, the drift error is in one dimension in the indoor of the building. However, the repetitiveness of this effect in other environments should be researched. In addition, the behavior of the drift error in time-series studies with SLAM LSs should be investigated in future research.

### Declaration of competing interest

The authors declare that they have no known competing financial interests or personal relationships that could have appeared to influence the work reported in this paper.

### Funding

This research was funded by Aalto University School of Engineering Tenure track (Digital Photogrammetry) funding, the Academy of Finland the Strategic Research Council projects, “Competence-Based Growth Through Integrated Disruptive Technologies of 3D Digitalization, Robotics, Geospatial Information, and Image Processing/Computing–Point Cloud Ecosystem” (No. 293389, 314312), Academy of Finland project “Quality4Roads” (No. 323783), project Profi5 “Autonomous systems” (No. 326246), the European Social Fund (S21997) and the European Regional Development Fund (No. A77489).

### References

- [1] Q. Wang, M.-K. Kim, Applications of 3D point cloud data in the construction industry: A fifteen-year review from 2004 to 2018, *Adv. Eng. Inform.* 39 (2019) 306–319, <http://dx.doi.org/10.1016/j.aei.2019.02.007>, URL <https://www.sciencedirect.com/science/article/pii/S1474034618304683>.
- [2] A.S. Rao, M. Radanovic, Y. Liu, S. Hu, Y. Fang, K. Khoshelham, M. Palaniswami, T. Ngo, Real-time monitoring of construction sites: Sensors, methods, and applications, *Autom. Constr.* 136 (2022) 104099, <http://dx.doi.org/10.1016/j.autcon.2021.104099>, URL <https://www.sciencedirect.com/science/article/pii/S0926580521005501>.
- [3] A. Keitaanniemi, J.-P. Virtanen, P. Rönholm, A. Kukko, T. Rantanen, M.T. Vaaja, The combined use of SLAM laser scanning and TLS for the 3D indoor mapping, *Buildings* 11 (9) (2021) 386, <http://dx.doi.org/10.3390/buildings11090386>, Publisher: Multidisciplinary Digital Publishing Institute URL <https://www.mdpi.com/2075-5309/11/9/386>.
- [4] G. Patrucco, F. Rinaudo, A. Spreafico, Multi-source approaches for complex architecture documentation: The “Palazzo Ducale” in Gubbio (Perugia, Italy), *Int. Arch. Photogram. Remote Sens. Spatial Inform. Sci.* (2019) <http://dx.doi.org/10.5194/ISPRS-ARCHIVES-XLII-2-W11-953-2019>.
- [5] P. Kim, J. Chen, Y.K. Cho, SLAM-driven robotic mapping and registration of 3D point clouds, *Autom. Constr.* 89 (2018) 38–48, <http://dx.doi.org/10.1016/j.autcon.2018.01.009>, URL <https://www.sciencedirect.com/science/article/pii/S0926580517303990>.
- [6] R. Otero, S. Lagüela, I. Garrido, P. Arias, Mobile indoor mapping technologies: A review, *Autom. Constr.* 120 (2020) 103399, <http://dx.doi.org/10.1016/j.autcon.2020.103399>, URL <https://www.sciencedirect.com/science/article/pii/S0926580520309791>.
- [7] G. Tucci, D. Visintini, V. Bonora, E.I. Parisi, Examination of indoor mobile mapping systems in a diversified internal/external test field, *Appl. Sci.* 8 (3) (2018) 401, <http://dx.doi.org/10.3390/app8030401>, Publisher: Multidisciplinary Digital Publishing Institute URL <https://www.mdpi.com/2076-3417/8/3/401>.
- [8] E. Farella, F. Menna, E. Nocerino, D. Morabito, F. Remondino, M. Campi, Knowledge and valorization of historical sites through 3d documentation and modeling, *ISPRS - Int. Arch. Photogram. Rem. Sens. Spatial Inform. Sci.* XLI-B5 (2016) 255–262, <http://dx.doi.org/10.5194/isprsarchives-XLI-B5-255-2016>.
- [9] T.J.B. Dewez, S. Yart, Y. Thuon, P. Pannet, E. Plat, Towards cavity-collapse hazard maps with Zeb-Revo handheld laser scanner point clouds, *Photogramm. Rec.* 32 (160) (2017) 354–376, <http://dx.doi.org/10.1111/phor.12223>, URL <https://onlinelibrary.wiley.com/doi/abs/10.1111/phor.12223>.
- [10] V. Frangez, B. Kramis, F. Hübscher, A. Baumann, Comparison of three innovative technologies for 3D-acquisition, modelling, and visualization of an underground mine, in: *FIG Congress 2018: Online Proceedings*, International Federation of Surveyors (FIG), 2018, p. 9502, Accepted: 2019-01-29T12:31:11Z URL <https://www.research-collection.ethz.ch/handle/20.500.11850/264109>.
- [11] S. Lagüela, I. Dorado, M. Gesto, P. Arias, D. González-Aguilera, H. Lorenzo, Behavior analysis of novel wearable indoor mapping system based on 3D-SLAM, *Sensors* 18 (3) (2018) 766, <http://dx.doi.org/10.3390/s18030766>, Publisher: Multidisciplinary Digital Publishing Institute URL <https://www.mdpi.com/1424-8220/18/3/766>.
- [12] V.V. Lehtola, H. Kaartinen, A. Nüchter, R. Kaijaluoto, A. Kukko, P. Litkey, E. Honkavaara, T. Rosnell, M.T. Vaaja, J.-P. Virtanen, M. Kurkela, A. El Issaoui, L. Zhu, A. Jaakkola, J. Hyyppä, Comparison of the selected state-of-the-art 3D indoor scanning and point cloud generation methods, *Remote Sens.* 9 (8) (2017) 796, <http://dx.doi.org/10.3390/rs9080796>, Publisher: Multidisciplinary Digital Publishing Institute URL <https://www.mdpi.com/2072-4292/9/8/796>.
- [13] A.C.T. So, L.L.Y. Pau, D. Jonas, B. Weigler, A pilot study on the use of handheld laser scanner for landform mapping and slope investigation in Hong Kong, 2015, p. 11, URL <https://citeseerx.ist.psu.edu/viewdoc/download?doi=10.1.1.740.4103&rep=rep1&type=pdf>.
- [14] C. Vanneschi, M. Eyre, M. Francioni, J. Coggan, The use of remote sensing techniques for monitoring and characterization of slope instability, *Procedia Eng.* 191 (2017) 150–157, <http://dx.doi.org/10.1016/j.proeng.2017.05.166>, URL <https://www.sciencedirect.com/science/article/pii/S187705817323068>.
- [15] C. Cabo, S. Del Pozo, P. Rodríguez-González, C. Ordóñez, D. González-Aguilera, Comparing terrestrial laser scanning (TLS) and wearable laser scanning (WLS) for individual tree modeling at plot level, *Remote Sens.* 10 (4) (2018) 540, <http://dx.doi.org/10.3390/rs10040540>, Publisher: Multidisciplinary Digital Publishing Institute URL <https://www.mdpi.com/2072-4292/10/4/540>.
- [16] S. Raval, B.P. Banerjee, S. Kumar Singh, I. Canbulat, A preliminary investigation of mobile mapping technology for underground mining, in: *IGARSS 2019 - 2019 IEEE International Geoscience and Remote Sensing Symposium*, 2019, pp. 6071–6074, <http://dx.doi.org/10.1109/IGARSS.2019.8898518>, ISSN: 2153-7003.
- [17] R. Zlot, M. Bosse, K. Greenop, Z. Jarzab, E. Juckes, J. Roberts, Efficiently capturing large, complex cultural heritage sites with a handheld mobile 3D laser mapping system, *J. Cult. Herit.* 15 (6) (2014) 670–678, <http://dx.doi.org/10.1016/j.culher.2013.11.009>, URL <https://www.sciencedirect.com/science/article/pii/S1296207413002185>.
- [18] A. Keitaanniemi, A. Kukko, J.-P. Virtanen, M.T. Vaaja, Measurement strategies for street-level SLAM laser scanning of Urban environments, *Photogram. J. Finland* 27 (1) (2020) <http://dx.doi.org/10.17690/020271.1>, URL [https://foto.aalto.fi/seura/julkaisut/pjf\\_e/pjf\\_e.html](https://foto.aalto.fi/seura/julkaisut/pjf_e/pjf_e.html).
- [19] J. Dai, L. Yan, H. Liu, C. Chen, L. Huo, An offline coarse-to-fine precision optimization algorithm for 3D laser SLAM point cloud, *Remote Sens.* 11 (20) (2019) 2352, <http://dx.doi.org/10.3390/rs11202352>, Publisher: Multidisciplinary Digital Publishing Institute URL <https://www.mdpi.com/2072-4292/11/20/2352>.
- [20] R. Milišaj, J. Oršulić, S. Bogdan, When measurements fail: using an interactive SLAM solution to fight bad odometry, in: *2020 IEEE International Instrumentation and Measurement Technology Conference, I2MTC, 2020*, pp. 1–6, <http://dx.doi.org/10.1109/I2MTC43012.2020.9129529>, ISSN: 2642-2077.
- [21] W. Liu, Z. Li, S. Sun, R. Malekian, Z. Ma, W. Li, Improving positioning accuracy of the mobile laser scanning in GPS-denied environments: An experimental case study, *IEEE Sens. J.* 19 (22) (2019) 10753–10763, <http://dx.doi.org/10.1109/JSEN.2019.2929142>, Conference Name: IEEE Sensors Journal.
- [22] C. Mezian, B. Vallet, B. Soheilian, N. Paparoditis, Uncertainty propagation for terrestrial mobile laser scanner, in: *The International Archives of the Photogrammetry, Remote Sensing and Spatial Information Sciences*, Vol. XLI-B3, Copernicus GmbH, 2016, pp. 331–335, <http://dx.doi.org/10.5194/isprs-archives-XLI-B3-331-2016>, ISSN: 1682-1750 URL <https://www.int-arch-photogram-remote-sens-spatial-inf-sci.net/XLI-B3/331/2016/>.
- [23] D. Barber, J. Mills, S. Smith-Voysey, Geometric validation of a ground-based mobile laser scanning system, *ISPRS J. Photogramm. Remote Sens.* 63 (1) (2008) 128–141, <http://dx.doi.org/10.1016/j.isprsjprs.2007.07.005>, URL <https://www.sciencedirect.com/science/article/pii/S0924271607000834>.
- [24] Q. Mao, L. Zhang, Q. Li, Q. Hu, J. Yu, S. Feng, W. Ochieng, H. Gong, A least squares collocation method for accuracy improvement of mobile LiDAR systems, *Remote Sens.* 7 (6) (2015) 7402–7424, <http://dx.doi.org/10.3390/rs70607402>, Publisher: Multidisciplinary Digital Publishing Institute URL <https://www.mdpi.com/2072-4292/7/6/7402>.

- [25] F. Abdulrahman, S. J. K. N., The importance of designing targets for improving the accuracy of mobile laser scanning data, 2014, URL [https://www.researchgate.net/publication/301776817\\_The\\_importance\\_of\\_designing\\_targets\\_for\\_improving\\_the\\_accuracy\\_of\\_Mobile\\_Laser\\_Scanning\\_data](https://www.researchgate.net/publication/301776817_The_importance_of_designing_targets_for_improving_the_accuracy_of_Mobile_Laser_Scanning_data).
- [26] F. Xi, D. Nancoo, G. Knopf, Total least-squares methods for active view registration of three-dimensional line laser scanning data, *J. Dyn. Syst. Meas. Control* 127 (1) (2004) 50–56, <http://dx.doi.org/10.1115/1.1876492>.
- [27] C.C. Marchant, T.K. Moon, J.H. Gunther, An iterative least square approach to elastic-Lidar retrievals for well-characterized aerosols, *IEEE Trans. Geosci. Remote Sens.* 48 (5) (2010) 2430–2444, <http://dx.doi.org/10.1109/TGRS.2009.2038903>, Conference Name: IEEE Transactions on Geoscience and Remote Sensing.
- [28] M. Leslar, B. Hu, J. Wang, Error analysis of a mobile terrestrial LiDAR system, *GEOMATICA* 68 (2014) 183–194, <http://dx.doi.org/10.5623/cig2014-303>.
- [29] M. Leslar, J. Wang, B. Hu, Bore-sight and lever arm calibration of a mobile terrestrial LiDAR system, *GEOMATICA* 70 (2) (2016) 97–112, <http://dx.doi.org/10.5623/cig2016-202>, Publisher: NRC Research Press URL <https://cdnsnciencepub.com/doi/10.5623/cig2016-202>.
- [30] D. Hauser, C. Glennie, B. Brooks, Calibration and accuracy analysis of a low-cost mapping-grade mobile laser scanning system, *J. Surv. Eng.* 142 (4) (2016) 04016011, [http://dx.doi.org/10.1061/\(ASCE\)SU.1943-5428.0000178](http://dx.doi.org/10.1061/(ASCE)SU.1943-5428.0000178), Publisher: American Society of Civil Engineers URL <https://ascelibrary.org/doi/abs/10.1061/%28ASCE%29SU.1943-5428.0000178>.
- [31] A. Habib, K.L. Bang, A.P. Kersting, D.-C. Lee, Error budget of Lidar systems and quality control of the derived data, *Photogramm. Eng. Remote Sens.* 75 (9) (2009) 1093–1108, <http://dx.doi.org/10.14358/PERS.75.9.1093>, URL <http://openurl.ingenta.com/content/xref?genre=article&issn=0099-1112&volume=75&issue=9&page=1093>.
- [32] J. Nolan, R. Eckels, A new method for validating mobile laser scanning (MLS) corridor surveys, *New South Wales* (2017) 13, URL <https://www.apas.org.au/files/conferences/2017/A-New-Method-for-Validating-Mobile-Laser-Scanning-MLS-Corridor-Surveys.pdf>.
- [33] J. Boavida, A. Oliveira, Precise long tunnel survey using the Riegl VMX-250 mobile laser scanning system, 2012, p. 13, URL [https://www.researchgate.net/publication/260922068\\_Precise\\_Long\\_Tunnel\\_Survey\\_using\\_the\\_Riegl\\_VMX-250\\_Mobile\\_Laser\\_Scanning\\_System](https://www.researchgate.net/publication/260922068_Precise_Long_Tunnel_Survey_using_the_Riegl_VMX-250_Mobile_Laser_Scanning_System).
- [34] J. Nolan, R. Eckels, M. Evers, R. Singh, M.J. Olsen, Multi-pass approach for mobile terrestrial laser scanning, *ISPRS Ann. Photogram. Remote Sens. Spatial Inform. Sci.* II-3/W5 (2015) 105–112, <http://dx.doi.org/10.5194/isprsannals-II-3-W5-105-2015>, URL <https://www.isprs-ann-photogramm-remote-sens-spatial-inf-sci.net/II-3-W5/105/2015/>.
- [35] H. Durrant-Whyte, T. Bailey, Simultaneous localization and mapping: part I, *IEEE Robot. Autom. Mag.* 13 (2) (2006) 99–110, <http://dx.doi.org/10.1109/MRA.2006.1638022>, Conference Name: IEEE Robotics Automation Magazine.
- [36] F. Di Stefano, S. Chiappini, A. Gorreja, M. Balestra, R. Pierdicca, Mobile 3D scan LiDAR: a literature review, *Geomat. Nat. Hazards Risk* 12 (1) (2021) 2387–2429, <http://dx.doi.org/10.1080/19475705.2021.1964617>, Publisher: Taylor & Francis eprint: <http://dx.doi.org/10.1080/19475705.2021.1964617>.
- [37] K. Cwian, M.R. Nowicki, J. Wietrzykowski, P. Skrzypczyński, Large-scale LiDAR SLAM with factor graph optimization on high-level geometric features, *Sensors (Basel, Switzerland)* 21 (10) (2021) 3445, <http://dx.doi.org/10.3390/s21103445>.
- [38] T. Emter, J. Peterleit, 3D SLAM with scan matching and factor graph optimization, in: *ISR 2018; 50th International Symposium on Robotics*, 2018, pp. 1–8, URL <https://publica.fraunhofer.de/handle/publica/403405>.
- [39] L. Huang, Review on LiDAR-based SLAM techniques, in: *2021 International Conference on Signal Processing and Machine Learning (CONF-SPML)*, 2021, pp. 163–168, <http://dx.doi.org/10.1109/CONF-SPML54095.2021.00040>.
- [40] Y. Chen, J. Tang, C. Jiang, L. Zhu, M. Lehtomäki, H. Kaartinen, R. Kaijaluoto, Y. Wang, J. Hyypä, H. Hyypä, H. Zhou, L. Pei, R. Chen, The accuracy comparison of three simultaneous localization and mapping (SLAM)-based indoor mapping technologies, *Sensors* 18 (10) (2018) 3228, <http://dx.doi.org/10.3390/s18103228>, Publisher: Multidisciplinary Digital Publishing Institute URL <https://www.mdpi.com/1424-8220/18/10/3228>.
- [41] G. Sammartano, A. Spanò, Point clouds by SLAM-based mobile mapping systems: accuracy and geometric content validation in multisensor survey and stand-alone acquisition, *Appl. Geomat.* 10 (4) (2018) 317–339, <http://dx.doi.org/10.1007/s12518-018-0221-7>.
- [42] A. University, Otakaari 4 | Aalto university, Otakaari 4 (2022) URL <https://www.aalto.fi/en/locations/otakaari-4>.
- [43] S. Cadge, Welcome to the ZEB revolution, *GEOmedia* 20 (3) (2016) URL <https://mediageo.it/ojs/index.php/GEOmedia/article/view/1326>.
- [44] M. Bosse, R. Zlot, P. Flicke, Zebedee: Design of a spring-mounted 3-D range sensor with application to mobile mapping, *IEEE Trans. Robot.* 28 (2012) 1104–1119, <http://dx.doi.org/10.1109/TRO.2012.2200990>.
- [45] A. Soininen, TerraScan user guide, 2021, URL <https://terrasolid.com/guides/tscan/index.html>.
- [46] D. Lague, N. Brodus, J. Leroux, Accurate 3D comparison of complex topography with terrestrial laser scanner: Application to the Rangitikei canyon (N-Z), *ISPRS J. Photogramm. Remote Sens.* 82 (2013) 10–26, <http://dx.doi.org/10.1016/j.isprsjprs.2013.04.009>, URL <https://www.sciencedirect.com/science/article/pii/S0924271613001184>.
- [47] GeoSLAM, Hub 6 user manual, 2022, URL <https://www.scribd.com/document/492851307/Hub-6-User-Manual>,
- [48] T. Fabry, D. Smeets, D. Vandermeulen, P. Suetens, 3D non-rigid point cloud based surface registration based on mean shift, *WSCG 2010: Full Papers Proceedings* (2010) 121–128, Conference Name: 8th International Conference in Central Europe on Computer Graphics, Visualization and Computer Vision in co-operation with EUROGRAPHICS URL [http://wscg.zcu.cz/WSCG2010/Papers\\_2010/!\\_2010\\_FULL\\_proceedings.pdf](http://wscg.zcu.cz/WSCG2010/Papers_2010/!_2010_FULL_proceedings.pdf).
- [49] GeoSLAM, ZEB go handheld 3D scanner: Laser scanning for everyone, 2022, URL <https://geoslam.com/solutions/zeb-go/>,
- [50] P. Rönholm, X. Liang, A. Kukko, A. Jaakkola, J. Hyypä, Quality analysis and correction of mobile backpack laser scanning data, *ISPRS Ann. Photogram. Rem. Sens. Spatial Inform. Sci.* III-1 (2016) 41–47, <http://dx.doi.org/10.5194/isprsannals-III-1-41-2016>, URL <http://www.isprs-ann-photogramm-remote-sens-spatial-inf-sci.net/III-1/41/2016/isprs-annals-III-1-41-2016.pdf>.
- [51] H. Jing, X. Meng, N. Slatcher, G. Hunter, Efficient point cloud corrections for mobile monitoring applications using road/rail-side infrastructure, *Surv. Rev.* 53 (378) (2021) 235–251, <http://dx.doi.org/10.1080/00396265.2020.1719753>, Publisher: Taylor & Francis.
- [52] B. Yang, Y. Li, X. Zou, Z. Dong, A marker-free calibration method for mobile laser scanning point clouds correction, *Int. Arch. Photogramm. Rem. Sens. Spatial Inform. Sci.* XLIII-B2-2020 (2020) 347–354, <http://dx.doi.org/10.5194/isprs-archives-XLIII-B2-2020-347-2020>, URL <https://www.int-arch-photogramm-remote-sens-spatial-inf-sci.net/XLIII-B2-2020/347/2020/>.